Clinical Cancer Research

Effects of Tumor Microenvironment Heterogeneity on Nanoparticle Disposition and Efficacy in Breast Cancer Tumor Models

Gina Song, David Darr, Charlene M Santos, et al.

Clin Cancer Res Published OnlineFirst September 17, 2014.

Title Page

Effects of Tumor Microenvironment Heterogeneity on Nanoparticle Disposition and Efficacy in Breast Cancer Tumor Models

Authors: Gina Song[1], David B. Darr[2], Charlene M. Santos [2,3], Mark Ross[3], Alain Valdivia[3], Jamie L. Jordan[2], Bentley R. Midkiff [2,4], Stephanie Cohen[4], Nana Nikolaishvili Feinberg[2, 4], C. Ryan Miller[2,5], Teresa K. Tarrant[2,6], Arlin B. Rogers[7], Andrew C. Dudley [2,8], Charles M. Perou [2,5,9], William C. Zamboni [1,2,10,11*]

Affiliations: [1]Division of Pharmacotherapy and Experimental Therapeutics, Eshelman School of Pharmacy, University of North Carolina (UNC) at Chapel Hill, [2]Lineberger Comprehensive Cancer Center, UNC at Chapel Hill, [3]The Animal Studies Core, UNC at Chapel Hill, [4]Translational Pathology Lab, UNC at Chapel Hill, [5]Department of Pathology and Laboratory Medicine, [6]Department of Medicine, Division of Rheumatology, Allergy, and Immunology and Thurston Arthritis Research Center, UNC at Chapel Hill, [7]Cummings School of Veterinary Medicine, Tufts University, [8]Department of Cell and Molecular Physiology, UNC at Chapel Hill, [9]Department of Genetics, UNC at Chapel Hill, [10]Carolina Center of Cancer Nanotechnology Excellence, UNC at Chapel Hill, [11]Center for Pharmacogenomics and Individualized Therapy, UNC at Chapel Hill.

***Corresponding Author:** William C. Zamboni, PharmD., PhD.

Division of Pharmacotherapy and Experimental Therapeutics

Eshelman School of Pharmacy

University of North Carolina at Chapel Hill

120 Mason Farm Road, suite 1013, CB 7361

Chapel Hill, NC 27599-7361

Office Phone: 919.843.6665

Office Fax: 919.966.5863

Email: zamboni@email.unc.edu

Grant Support: The study was supported by the University Cancer Research Funding (UCRF) and Award Number UL1RR025747 from the National Center for Research Resources. The content is solely the responsibility of the authors and does not necessarily represent the official views of the National Center for Research Resources or the National Institutes of Health.

Conflict of Interest: The authors declare no competing financial interest.

Running title: Tumor microenvironment and nanoparticles in breast cancer

Abstract: 249

Text: 5,000

Total number of figures and tables: 6

Keywords: Tumor microenvironment, Breast cancer, Pharmacokinetics, Pharmacodynamics, Nanoparticle

Statement of Translational Relevance

Nanoparticle (NP)-based therapy exploits the enhanced permeability and retention (EPR) effects of the abnormal tumor microenvironment and has proved to selectively target tumor cells and reduce the unwanted toxicities in normal cells. However, only few nanomedicines have been approved and used clinically due to limited impacts on overall survival. Heterogeneity of the tumor microenvironment has been observed within and between human tumor types, but its effects on the variable delivery and efficacy of nanomedicines have not been extensively investigated. In this study, we report that heterogeneous tumor microenvironment and/or tumor cell features correlated with significantly different tumor delivery and efficacy of polyethylene glycol tagged (PEGylated) liposomal doxorubicin, but not doxorubicin, between two intrinsic murine breast tumor subtypes. This finding implicates that profiling of the tumor and the microenvironment and selection of patients with tumors conducive to the NPs are required for the optimal delivery and therapeutic outcomes for NP-based therapy.

ABSTRACT

Purpose: Tumor cells are surrounded by a complex microenvironment. The purpose of our study was to evaluate the role of heterogeneity of the tumor microenvironment in the variability of nanoparticle (NP) delivery and efficacy.

Experimental designs: *C3(1)-T-Antigen* genetically engineered mouse model (C3-TAg) and *T11*/*TP53*^{Null} orthotopic syngeneic murine transplant model (T11) representing human breast tumor subtypes basal-like and claudin-low, respectively, were evaluated. For the pharmacokinetic studies, non-liposomal doxorubicin (NL-doxo) or polyethylene glycol tagged (PEGylated) liposomal doxorubicin (PLD) was administered at 6 mg/kg intravenously (IV) x1. Area-under-the concentration versus time curve (AUC) of doxorubicin was calculated. Macrophages, collagen, and the amount of vasculature were assessed by immunohistochemistry. Chemokines and cytokines were measured by multiplex immunochemistry. NL-doxo or PLD was administered at 6 mg/kg IV weekly x6 in efficacy studies. Analyses of intermediary tumor response and overall survival were performed.

Results: Plasma AUC of NL-doxo and PLD encapsulated and released doxorubicin were similar between two models. However, tumor sum total AUC of PLD was 2-fold greater in C3-TAg compared with T11 (P<0.05). T11 tumors showed significantly higher expression of CC chemokine ligand (CCL) 2 and vascular endothelial growth factor (VEGF)-a, greater vascular quantity, and decreased expression of VEGF-c compared to C3-TAg (P<0.05). PLD was more efficacious compared to NL-doxo in both models.

Conclusion: The tumor microenvironment and/or tumor cell features of breast cancer affected NP tumor delivery and efficacy, but not the small molecule drug. Our findings reveal the role of the tumor microenvironment in variability of NP delivery and therapeutic outcomes.

INTRODUCTION

There have been major advances in nanotechnology for targeted delivery of pharmacologic agents to sites of disease, such as cancer (1, 2). In oncology, nanoparticle (NP)-based therapies exploit the enhanced permeability and retention (EPR) effect caused by the unique vascular structure of solid tumors (i.e., hypervasculature and defective lymphatic drainage) (3). The EPR effect is a key rationale that advances the use of NPs for treatment of cancer and renders the preferential delivery and accumulation of NPs to the tumor cells (3). This allows nanomedicines to have advantages over conventional medicines including prolonged circulation, selective delivery of entrapped drug to tumor, and improved therapeutic index (4). However, there is limited data on the heterogeneity and factors affecting the EPR in preclinical tumor models and, especially, solid tumors in patients to correlate these factors with the highly variable clinical responses of NP-based therapies (5).

It has been shown that NPs have immunological properties that may stimulate or suppress the immune system (5, 6). NPs can interact with immune components in blood, which influences the uptake and clearance by the mononuclear phagocyte system (MPS), and potentially biodistribution and delivery to the targeted site such as tumors (7, 8). Previously, we have reported that the variability in the pharmacokinetics (PK) and pharmacodynamics (PD) of nanomedicines such as Doxil® (PEGylated liposomal doxorubicin; PLD) and S-CKD602 (PEGylated liposome of CKD-602, a camptothecin analog) is associated with patient age, gender, and the function of circulating monocytes in plasma of patients with solid tumors (9-11). We also showed a bidirectional interaction between SCKD-602 and circulating monocytes in patients with solid tumors (12). However, these factors may not sufficiently explain the high variability in the PK and PD of NP-based therapies in patients with solid tumors.

Solid tumors are characterized by a complex and unique microenvironment that consists of infiltrating immune cells such as tumor-associated macrophages (TAMs), a variety of growth factors, chemokines and cytokines, dense interstitial matrix, and the abnormal blood and lymphatic vascular structure (13, 14). These factors interplay with the tumor cells to modify the tumor microenvironment and promote tumor progression (13, 14). It has been reported that there is intra- and inter-tumor variability in the tumor cells and the microenvironment that results in the heterogeneity of molecular, pathological, and clinical features of each tumor type (15-17). Studies have revealed that abnormal vascular architecture and dense collagen matrix can act as environmental barriers hindering the delivery of NPs and result in suboptimal clinical outcomes (17). Previously, we have also reported that increased tumor delivery and release of CKD-602 from S-CKD602 in SKOV-3 ovarian xenografts compared with A375 melanoma xenografts correlated with increased expression of CD11c positive dendritic cells (DCs) in the tumors, suggesting that the variability in NP tumor disposition may be associated with the phagocytic cells (i.e., DC and TAMs) (18). Given the heterogeneity of the tumor microenvironment between and within human cancer types and its potential impacts on the tumor delivery and therapeutic outcomes of NP-based therapy, it is imperative to evaluate the roles of the microenvironment factors and their interaction with NPs in a systemic manner for the optimal delivery and efficacy of nanomedicines (5, 17).

Genetically engineered mouse models (GEMMs) and orthotopic syngeneic murine transplant (OST) have proven to be valuable experimental models for discovery of biomarkers and prediction of chemotherapy responses in human cancers (19, 20). RNA expression profiling of 13 distinct GEMMs of breast cancer identified mouse models that faithfully represent human intrinsic breast tumor subtypes including Basal-like (*C3(1)-T-Antigen* (C3-TAg)) (21) and

Claudin-low (*T11/TP53*$^{-/-}$ (T11)) (22). No single claudin-low GEMM was found, but orthotopic syngeneic transplantable tumors from a BALB/c *TP53*^{Null} mouse was shown to faithfully recapitulate the human claudin-low expression phenotype (22). Basal-like subtype (C3-TAg) is characterized by high expression of basal gene expression features and the proliferation signature (19, 21). The majority of these tumors are clinically estrogen receptor (ER) negative, progesterone receptor (PR) negative, and HER2-negative (triple negative breast cancer), which leads to lack of validated biological targets and poor responses to current chemotherapies (19, 21). The majority of claudin-low (T11) tumors are also triple negative breast tumors with poor prognosis but were shown to have lower pathological complete response (pCR) rate to anthracycline/taxane-based chemotherapies compared to basal-like tumors (23). Claudin-low T11 tumors exhibited distinguishing gene expression characteristics (i.e. more enriched in immune system responses and endothelial cell-like signature) as well as histological phenotypes (i.e. endothelial/tube-like morphology and high vascular permeability) compared to basal-like C3-TAg tumors (23, 24).

Here, we used the genomically validated basal-like C3-TAg and claudin-low T11 murine breast tumor models to test our hypothesis that the heterogeneity of the tumor cells and the tumor microenvironment between breast tumor subtypes affect the tumor delivery and therapeutic outcomes of NP. We evaluated PEGylated liposomal doxorubicin (PLD; Doxil®) which has been used for treatment of metastatic breast cancer and non-liposomal doxorubicin (NL-doxo; Adriamycin®) as a comparator (25). Furthermore, we examined the dynamic modulation of the tumor physiology, such as TAMs, collagen, tumor vasculature, and chemokines, after treatment with each agent in these mouse models.

MATERIALS AND METHODS

Treatments. PLD was purchased from FormuMax Scientific (Palo Alto, CA) (Supplementary Table S1) and diluted with 5% dextrose to 1.2 mg/mL prior to injection. NL-doxo was purchased from Sigma Aldrich (St. Louis, MO) and diluted with 0.9% NaCl to 1.2 mg/mL prior to injection.

Animal Models. *In vivo* experiments were performed with the approval of University of North Carolina at Chapel Hill's Institutional Animal Care and Use Committee (IACUC). GEMM of strain of FVB/n carrying a transgene for *C3(1)SV40 T-antigen* (C3-TAg) were bred in-house and observed until the tumor size was met (> 0.5 cm) in any dimension (21). Tumors derived from *BALB/c TP53*$^{-/-}$ orthotopic mammary gland transplant line (T11) was transplanted into the inguinal mammary fat pad of 12 week old wild-type BALB/c mice (Jackson Labs, strain 000651) (19). Mice were housed in the UNC Lineberger Comprehensive Cancer Center's Mouse Phase I Unit (MP1U) and observed for tumors as per standard practice (22). Mice were randomized to treatment cohorts and therapy began once a tumor reached 60-100 mm^3.

PK Studies in Plasma, Tissues, and Tumor. NL-doxo and PLD were administered at 6 mg/kg (doxorubicin equivalent) IV x1 via a tail vein. Mice (n=3) were euthanized prior to and at 0.083, 0.5, 1, 3, 6, 24, 48, 72, and 96 h after administration of each drug. Each blood sample was processed to evaluate encapsulated and released doxorubicin in plasma as described previously (18, 26). In the same mice, liver, spleen, lung, and tumors were collected, preserved by snap freezing, and stored at – 80°C. To measure the sum total (encapsulated and released) doxorubicin in tumors and tissue samples, samples were thawed on ice, weighed, and homogenized with pH 7.4 PBS buffer (1g tissue: 3mL PBS) using a Precellys (13-RD000) 24 bead mill homogenizer (Omni International, Inc.). Doxorubicin concentration was determined using an existing high

performance liquid chromatography-fluorescence (HPLC-FL) assay (18, 26). Noncompartmental PK analyses of NL-doxo and PLD in plasma, tumor, and tissues were performed using Phoenix v.6.2 (Pharsight Corp., CA). The area under the concentration versus time curve from 0 to t (AUC_{0-t}) was calculated using the linear up and log down rule.

Immunohistochemistry (IHC) and Digital Imaging. Tumor samples were collected at necropsy, fixed overnight in 10% neutral-buffered formalin, processed routinely, and stained with hematoxylin and eosin (H&E). IHC for F4/80 (TAM), collagen IV, and CD31 (endothelial cells) were performed as well (27). Further information is described in Supplementary Data.

Morphometric Quantitation of Macrophages, Collagen, and Microvessel Density (MVD). Whole tumor images were captured using an Aperio slide scanner at the UNC Translational Pathology Laboratory. F4/80+ macrophages were classified into three groups: (a) peritumoral/peripheral - capsule; (b) intratumoral - viable; and (c) intratumoral – necrotic (Supplementary Fig. S1) (28, 29). For scoring collagen IV semi-quantitatively, H-scores were generated by the Aperio color deconvolution methods. MVD was calculated by number of vessels divided by stained areas (mm^2) using the Definien Tissue Studio software (Munich, Germany) (30). The physiologic state of the vasculature including the size and open lumen status was assessed in representative vascularized areas within tumor (Supplementary Fig. S2). Collagen and MVD were assessed in capsule and viable tumor only. Further information is described in Supplementary Data.

Multiplex-bead Array Assay. Mouse Cytokine/Chemokine Magnetic Bead Panel was purchased from Milipore (Billerica, MA). The 96-well plate kit was customized to measure CC chemokine ligand (CCL) 2, also known as monocyte chemoattractant protein-1 (MCP-1), and CC chemokine ligand (CCL) 5, also known as regulated on activation, normally T-cell expressed

and secreted (RANTES), in plasma and tumor and vascular endothelial growth factor-a (VEGF-a) and VEGF-c in tumor (14, 30). Further information is described in Supplementary Data.

Efficacy Studies. Once tumor mass reached 60-100 mm^3, mice were randomized into treatment groups. NL-doxo and PLD were administered at 6 mg/kg x1 weekly for 6 weeks. Tumors were measured using calipers daily and tumor volume was calculated as (*Volume = [(width)^2 x length]/2*). Treatment outcome was assessed as intermediary tumor volume and tumor growth inhibition (TGI %) (31). TGI was calculated from the following formula: TGI (%) = (1-T/C) x 100, where T indicates the mean final tumor volume (mm^3) of the treatment group and C indicates the mean final tumor volume (mm^3) of the control group (31). Survival was monitored individually and mice were euthanized for tumor ulceration, tumor size of 2 cm in any dimension with single tumor, or 1.3 cm in any dimension with multiple tumors.

Statistical Analysis. Statistical analyses were carried out using SAS v.9.2 (Cary, NC) and Prism5 software (GraphPad Software, Inc.). Equality of AUC between C3-TAg model and T11 model was tested with Nedelman's modification of the Bailer method for sparse samples, using a two-sample t-test (32). Analysis of covariance (ANCOVA) with baseline tumor volume as covariate was performed followed by adjustment for multiple comparisons using Holm test to test intermediary tumor volume among treatment groups (33). Kaplan-Meier (KM) survival curves were plotted, and the difference in overall survival between the groups was analyzed by the log-rank test. *P* value of less than 0.05 was considered statistically significant. All statistical tests were two-sided.

RESULTS

Plasma, Tissue, and Tumor Disposition of NL-doxo and PLD. To predict plasma, tissue, and tumor disposition of NL-doxo and PLD in human basal-like and claudin-low breast tumor subtypes, we performed the PK studies of NL-doxo and PLD in their murine counterparts, C3-TAg model and T11 model, respectively. Plasma, tissues, and tumor doxorubicin concentration versus time profiles after administration of NL-doxo or PLD at 6 mg/kg IV x 1 are presented in Fig. 1. AUC from 0 to 96 h, a measured index of the total doxorubicin exposure over time, was calculated by noncompartmental PK analysis. PK parameters for both treatments are presented in Supplementary Table S2.

The doxorubicin $AUC_{0\text{-}96h}$ in plasma, tissues, and tumors after NL-doxo administration were similar between two models (P>0.05) (Fig. 1A, 1C, 1D, 1E, and 1F). In PLD treated mice, both plasma encapsulated (the drug within the liposomal carrier) and released (active-drug released from the liposomal carrier) doxorubicin $AUC_{0\text{-}96h}$ were similar in the two models (Fig. 1B). However, after PLD administration, the sum total (encapsulated + released) doxorubicin $AUC_{0\text{-}96h}$ in tumors was 2-fold greater in C3-TAg compared to T11 (480 ± 71 versus 210 ± 30 μg·h/g, respectively; P=0.012) (Fig. 1C and Supplementary Table S2). The doxorubicin accumulation in the liver was 1.5-fold higher in T11 compared to C3-TAg after PLD administration (687 ± 61 versus 438 ± 18 μg·h/g, respectively; P=0.002) (Fig. 1D). The doxorubicin accumulation in the spleen and the lung was similar between C3-TAg and T11 after NL-doxo and PLD administration (Fig. 1E and 1F). These data suggest that heterogeneity of the tumor microenvironment and/or tumor cell features between C3-TAg and T11 models affected PLD tumor delivery and distribution to the liver, but not NL-doxo.

Tumor-Associated Macrophages (TAMs). To evaluate the effects of TAMs on the delivery of NL-doxo and PLD and characterize the interaction with these drugs, C3-TAg tumors and T11 tumors from the PK studies were stained for F4/80 (Fig. 2). At baseline, most TAMs were located in the hypoxic necrotic area and the periphery (capsule) with lower numbers present in viable tumor in both models (Supplementary Table S3). There was no significant difference in the baseline level of TAMs in all sub-regions between two models.

However, the time profile of TAMs over 96 h was distinguished between after NL-doxo and PLD administration (Fig. 3). The changes in the TAM infiltration after NL-doxo administration were inconsistent between C3-TAg and T11 models (Fig. 3A and 3C). In contrast, after PLD, a nadir occurred at 24 h followed by TAM infiltration in both models (Fig. 3B and 3D). The % decrease at nadir (24 h) in TAMs localized in the viable tumors was greater in T11 compared to C3-TAg (37.2% vs. 6.6%, $P>0.05$) (Fig. 3B and 3D). The $AUC_{0\text{-}96h}$ of F4/80 H-score, an indicator of total influx of TAMs, was similar between C3-TAg model and T11 model after administration of NL-doxo and PLD (Supplementary Table S3).

CCL2 and CCL5 in Tumors and Plasma. CCL2 and CCL5 are overexpressed in human and murine breast tumors and play a central role in mobilization of monocytes into tumors and differentiation into TAMs (14, 34). To evaluate whether these chemokines are associated with tumor delivery of PLD or NL-doxo *in vivo*, we measured intratumoral concentrations of CCL2 and CCL5 at 0, 24, 48, and 96 h after PLD or NL-doxo administration using multiplex chemokine assay.

Baseline CCL2 concentration was 5-fold higher in T11 tumors than C3-TAg tumors (18 ± 1.5 versus 3.8 ± 0.5 ng/g: mean ± SEM (n=4 for each model), respectively) ($P<0.0001$) (Fig. 4A). CCL2 concentration in tumors increased over 96 h to a greater extent after PLD compared to

NL-doxo in both models (Fig. 4A). Interestingly, it was noted that the time profile of CCL2 in tumors resembled the time course of TAMs after NL-doxo and PLD in T11 (Fig. 3C, 3D, and 4A). In plasma, baseline CCL2 concentrations were 2-fold higher in T11 compared to C3-TAg (148 ± 49 versus 74 ± 8 ng/mL, respectively) (P=0.19) (Fig. 4B). Plasma CCL2 concentration was significantly increased at 96 h after PLD in C3-TAg model (P=0.023), but little was changed in T11 model (Fig. 4B).

In contrast to CCL2, there was no difference in baseline CCL5 tumor concentrations between two models (0.5 ± 0.1 versus 0.4 ± 0.1 ng/g: mean ± SEM) (Fig. 4C). After PLD administration, there was a noticeable increase in CCL5 tumor concentrations at 96 h in T11 model (P=0.002), but a high variability was observed at 96 h in C3-TAg model (P=0.24) (Fig. 4C). In plasma, baseline CCL5 concentrations were similar between two models. Little change was observed in plasma CCL5 concentration after PLD or NL-doxo administration in both models (Fig. 4D).

Next, we assessed the total amount of chemokine produced in tumors after PLD or NL-doxo administration by calculating the AUC from 0 to 96 h, a measured index of the total amount of a chemokine produced over time. CCL2 $AUC_{0\text{-}96h}$ was significantly greater in T11 tumors compared with C3-TAg tumors after PLD administration (707 ± 119 versus 2,332 ± 235 ng·h/g: mean ± SEM; P=0.0008) and NL-doxo (406 ± 76 versus 1,505 ± 218 ng·h/g; P=0.003) (Fig. 4A). However, there was no difference in plasma CCL2 $AUC_{0\text{-}96h}$, plasma CCL5 $AUC_{0\text{-}96h}$, and tumor CCL5 $AUC_{0\text{-}96h}$ between two models (Fig. 4B, C, and D). Together, these data indicate that there was an inverse relationship between the levels of intratumoral CCL2 expression and tumor delivery of PLD. Moreover, PLD showed to induce CCL2 expression in tumors to a greater extent than NL-doxo and the increase was more pronounced in T11 model compared to C3-TAg model.

Collagen and the Vasculature in Tumors. To assess the effects of tumor physiology on the tumor delivery of NL-doxo and PLD, tumors at baseline were stained for extracellular collagen matrix (collagen IV) and the quantity and physiologic state of the vasculature (CD31) (Fig. 2). We also evaluated the changes from baseline at 96 h after NL-doxo or PLD administration to characterize the interaction between the drugs and these factors.

H-score of collagen at baseline was 1.5-fold greater in C3-TAg than T11 (82 ± 13 versus 53 ± 24, respectively; $P>0.05$). Collagen expression tended to modestly increase after administration of NL-doxo and PLD in both models except in T11 tumors treated with NL-doxo ($P>0.05$) (Supplementary Fig. S3).

The baseline vascular quantity measured by MVD score was significantly greater in T11 tumors compared to C3-TAg tumors (933 ± 65 versus 691 ± 67 mean MVD ± SEM, respectively) ($P=0.04$) (Fig. 5A). Most of the blood vessels identified were small (~87%), followed by medium (12%) and large (1%) in both models (Supplementary Fig. S4). In addition, a significantly greater number of blood vessels in T11 tumors were shown to have open lumen compared to C3-TAg tumors ($P=0.01$), indicating hyperperfusion and hyperpermeability of the vasculature in T11 tumors (Fig. 5B). After administration of NL-doxo or PLD, the vascular quantity in C3-TAg tumors did not change over time (Fig. 5C); however, there was a 31 % decrease in MVD score from baseline to 96 h after PLD in T11 tumors (933 ± 65 at 0 h versus 555 ± 69 at 96 h: mean MVD ± SEM; $P>0.05$) (Fig. 5D).

Vascular Endothelial Growth Factors (VEGF) in Tumors. VEGF-a and VEGF-c are known for their central role in angiogenesis and lymphangiogenesis in the tumor microenvironment, respectively (30). As these growth factors play a crucial role in determining vascular permeability, lymphatic drainage of fluid from tumors, and EPR effects, intratumoral

VEGF-a and VEGF-c were measured to examine the impacts on transvascular transport of NL-doxo and PLD. At baseline, VEGF-a was approximately 7-fold higher in T11 tumors than C3-TAg tumors (11 ± 1.6 versus 1.5 ± 1.2 ng/g: mean ± SEM; *P*=0.003) (Fig. 5E). VEGF-c was 2-fold higher in C3-TAg tumors compared to T11 tumors at baseline (2.3 ± 0.4 versus 1.1 ± 0.1 ng/g) (*P*=0.03) (Fig. 5F).

To explore the effects of PLD and NL-doxo on angiogenesis in different breast tumor subtypes, we evaluated the modulation of these pro-angiogenic factors over time after each drug treatment. Surprisingly, the effects of PLD and NL-doxo on expression of VEGF-a and VEGF-c appeared to vary with breast tumor subtypes. After PLD administration, VEGF-a in T11 tumors was steadily decreased in T11 but increased in C3-TAg tumors (*P*=0.02) (Fig. 5E). This finding was consistent with the changes seen in the MVD score after PLD administration (Fig. 4E and 4F). PLD significantly reduced VEGF-c in C3-TAg tumors (*P*=0.02), but elevated it in T11 tumors (*P*=0.05) (Fig. 5F). NL-doxo also altered the expression of VEGF-a and VEGF-c in both models, but to a lesser extent compared to PLD (Fig. 5E and 5F). These results suggest that T11 tumors exhibit hypervascularization and impaired lymphatic functions compared to C3-TAg tumors as demonstrated by higher VEGF-a and lower VEGF-c, which may hamper the tumor delivery of PLD (13, 17). In addition, PLD demonstrated anti-angiogenic effects and pro-lymphangiogenic effects on T11 tumors, which may return the vasculature to more normal phenotype over 96 hour, but not on C3-TAg tumors (17, 35).

Efficacy. In order to evaluate the effectiveness of PLD or NL-doxo in C3-TAg and T11 breast tumors, we performed the efficacy studies using no treatment (NT), NL-doxo, and PLD. With a null hypothesis of equal tumor growth with a chemotherapeutic agent in two groups of murine breast tumor models, 15 mice per group give 80% power to detect a difference of 1.06 SD at

two-sided α level of 0.05 based on error estimates from previous study results (20). We tested 20 mice per treatment group for each mouse model to have an appropriate power to detect a difference in responses.

Intermediary tumor volume at 21 days for C3-TAg model and at 14 days for T11 model was used to quantify the therapeutic responses. The 21 day and 14 day response for each model was chosen as the primary response endpoint based on the fact that 50% of the untreated animals did not survive past 21 days for C3-TAg model and 14 days for T11 model. The median and range of survival days of untreated C3-TAg and T11 mice were 20 (12-47) and 15 (14-20), respectively (20).

Mean tumor growth is presented in Fig. 6A and 6B. Mean tumor volume comparison indicated that PLD was more efficacious at inhibiting the growth of both breast tumors compared to no treatment or NL-doxo (P=0.013 and P<0.0003, respectively). TGI% of NL-doxo and PLD was 34.6 and 56.8 in C3-TAg model, and 29.6 and 76.3 in T11 model, respectively, which indicates that T11 tumors may be slightly more responsive to PLD compared to C3-TAg tumors (Fig. 6C and 6D). KM plots are presented in Fig. 6E and 6F. PLD significantly prolonged the survival of C3-TAg models (P<0.0001), but modestly in T11 models (P=0.083) compared with no treatment and NL-doxo. However, it should be noted that T11 tumors treated with PLD became ulcerative in 18 days post treatment and were terminated in accordance to IACUC guidelines as a humane endpoint for the study. Ulceration is a lesion typified by a necrosis of tissues, which may reflect responses of T11 tumors to PLD (36). Thus, the results of overall survival for T11 mice treated with PLD may not reflect the accurate survival outcomes.

DISCUSSION

Heterogeneity in tumor cells and/or the tumor microenvironment observed within and between tumor types is suggested to be a contributing factor to inefficient transport of nanomedicines to tumors, but there are limited preclinical and clinical data to understand the mechanisms and correlate the varying clinical responses to nanomedicines (5, 9, 11).

We used genomically validated murine breast tumor models and demonstrated that tumor delivery of PLD was significantly greater in the basal-like C3-TAg model compared to the claudin-low T11 model (P=0.012), whereas the difference in tumor delivery was not seen with NL-doxo. In addition, claudin-low T11 tumors were more responsive to PLD compared to basal-like C3-TAg tumors. To evaluate which tumor-associated factors may contribute to the variable tumor delivery and efficacy of PLD in breast tumor subtypes, we assessed the physiological factors that have shown to be associated with NP transportation into and within tumors, including TAMs, collagen, and blood and lymphatic vasculature as well as chemokines (13, 14, 17)

TAMs are major leukocytes recruited into murine and human tumors by chemoattractants and educated by the tumor microenvironment to promote tumor progression (13, 29). Macrophages have been shown to be involved in phagocytosis and clearance of NPs (7, 8, 10, 11) and to promote delivery of NPs into tumors serving as a “Trojan Horse” (37). Based on the evidence, we evaluated TAMs in association with tumor delivery and efficacy of PLD compared to NL-doxo in two breast tumor subtypes. The baseline level of TAMs were similar between two models, which indicates that the level of TAMs may not account for the variable tumor delivery of PLD in these breast tumor subtypes (38, 39). However, the different changes of TAMs over time after NL-doxo or PLD in two models implicate the drug- and tumor-dependent interaction

between TAMs and drugs. Consistent with the data generated in studies by our group and others, our finding indicates that uptake of PLD by TAMs may lead to cytotoxicity and cause a temporal decrease in the number of TAMs (12, 40). Further experiments using microscopy-based approaches will help confirm PLD uptake by TAMs and subsequent cytotoxic effects on the cells.

Recruitment of TAMs to solid tumors is regulated by chemokines, in particular CCL2, secreted by both malignant and stromal cells (14, 41). Hence, the system of CCL2 and its major receptor CCR2 has been shown to promote tumor cell survival and motility (42), metastasis (43), and angiogenesis (41). In addition, induction of CCL2 expression and CCL2-mediated monocyte/myeloid cell recruitment have shown to mediate therapeutic anticancer immune response elicited by immunogenic chemotherapy (i.e. doxorubicin) (44) and counteract the antitumor effects of vascular-targeted therapies (i.e. VEGF inhibitor) as a compensatory mechanism (45, 46). Consistent with these observations, the expression of CCL2 in both C3-TAg tumors and T11 tumors was increased after NL-doxo and, to a greater extent, after PLD, suggesting that PLD is more immunogenic compared to NL-doxo (6, 7). In addition, in T11 tumors where PLD exhibited anti-angiogenic effects, PLD-mediated induction of CCL2 expression was significantly greater compared to C3-TAg tumors (45, 46).

In addition to cancer, CCL2 is also well studied for its chemotactic effects, activation of stellate cells, and angiogenesis in acute and chronic liver inflammation (47). Given that cancer can be considered as a chronic inflammatory disease, it is possible that elevated plasma CCL2 may serve as an inflammatory stimulus to monocytes and influence the migration and infiltration of macrophages to liver, spleen, and other organs (48). NP transport may be enhanced via increased angiogenesis, which influences the uptake by macrophages in the affected organs (8,

39, 47, 48). This may explain the greater accumulation of PLD in the liver and spleen from the T11 model compared to the C3-TAg model. However, to confirm this possibility, further experiments to assess hepatic blood vessels and the function of macrophages in these organs before and after PLD administration are needed.

The tumor interstitial spaces comprise a densely interconnected network of collagen fibers that interact with proteoglycans and glycosaminoglycans (17). The interstitial transport of liposomes via diffusion is determined by collagen content and substantially blocked due to interactions with collagen matrix (17). In our studies, the baseline level of collagen was similar between two breast tumor subtypes and the changes in collagen after NL-doxo or PLD were not noticeable. These data suggest that collagen matrix may not account for different tumor delivery of PLD between two murine breast tumor models. Further experiments are warranted to validate the effects of interstitial collagen matrix on the transport of PLD in tumors and interaction between collagen and PLD.

The ratio of tumor to plasma $AUC_{0\text{-}96h}$ of PLD in C3-TAg model and T11 model was 0.30 and 0.15, respectively, which suggests that the efficiency of transvascular transportation of PLD into tumor is 2-fold higher in C3-TAg model. These findings led us to measure the amount and physiologic state of the vasculature and pro-angiogenic factors for blood microvascular endothelial cells (VEGF-a) and lymphatic endothelial cells (VEGF-c) in these models. Interestingly, claudin-low T11 tumors exhibit features of hypervascularization and inefficient lymphatic networks, which may increase interstitial fluid pressure (IFP) (17) and hamper the transvascular transport of PLD (17, 49). Consistent with our findings, RNA expression profiling of more than 3,000 human breast tumors showed that claudin-low tumors had the highest vasculature signature expression compared to any of the other breast tumor subtypes (24). In

addition, claudin-low tumor cell lines exhibited endothelial cell-like tube morphology with high vascular permeability compared to other breast tumor subtypes (24).

The interactions between PLD and the tumor vasculature were different between two breast tumor subtypes. PLD exhibited normalizing effects on the blood and lymphatic vessels over 96 h and decreased the vascular density (MVD score) by 30% in claudin-low T11 tumors; however, no such changes were observed in basal-like C3-TAg tumors. Consistent with our finding, it has been reported that Doxil treatment exerted strong tumor growth inhibitory effects in B16.F10 melanoma-bearing mice as well as strongly reduced the intratumoral level of VEGF-a, which is produced in high amounts by melanoma cells (38). After clodronate-containing long circulating liposome (LCL), known for its TAM-suppressive effects, a significantly strong additional antitumor effect was observed after Doxil administration compared to that induced by clodronate-LCL; however, no additional strong reducing effect on VEGF-a was reported (38). This indicated that Doxil mainly acts via direct cytotoxic effects on tumor cells with slightly suppressing effects on TAM-mediated angiogenesis (38). Based on this observation, T11 tumor-specific VEGF-a suppressing effect of PLD may be associated with greater responsiveness of T11 tumors to PLD. *In vitro* studies assessing IC50 of PLD in human basal-like cells and claudin-low cells would further confirm the different sensitivity to PLD between two breast tumor types.

The fact that T11 is an OST model compared to C3-TAg GEMM may play a role as confounding factor in our study despite the conserved gene expression features between murine T11 OST tumors and human claudin-low tumors (19, 23, 24). However, the clinical relevance of our results from T11 OST models can be justified on the basis of the evidence showing that gene expression signatures derived from chemotherapy-treated T11 models successfully predicted the

pathological complete response to anthracycline/taxane therapy in human patients with breast cancer (20, 23). The background difference between two murine models may confound the breast tumor subtype-specific difference in PLD delivery and further studies are warranted to evaluate potential effects. Our findings may not be applicable to other NP platforms with different targeting strategies and/or surface characteristics (i.e., passive targeting vs. active targeting, lipid versus polymeric) (1, 2, 4, 17). Jain *et al* reported that vessel normalization with anti-angiogenic therapies improved the delivery and effectiveness of small NP (diameter, 12 nm) but not large NP (125 nm), emphasizing the importance of optimization of both NP and the tumor microenvironment (50). Thus, it is critical to profile the tumor microenvironment within and between tumor types and select patients with tumors that are likely to respond to NP-based therapies (5, 17).

Studies have reported that breast tumor classification based on gene expression profiling adds significant prognostic and predictive information to standard parameters (i.e. hormone receptor status, tumor size and grade, and node status etc.) for patients with breast cancer (16, 19-24). Intrinsic human and murine breast tumor subtypes have shown different sensitivities to chemotherapies including neoadjuvant anthracycline/taxane-based treatment (19, 20, 23). In line with that, we demonstrated that the biologic heterogeneity of breast tumors may affect the delivery and efficacy of NP-based therapies in murine models and not all breast tumors may be uniformly conducive to NP therapies. Our findings suggest that PLD and other NP-based therapies for breast cancer need to be evaluated with respect to the heterogeneity of breast tumors in the retrospective and prospective studies.

Authors' Contributions:

Conception and design: G. Song, W.C. Zamboni

Development of methodology: G. Song, B.R. Midkiff, S. Cohen, N. N. Feinberg, A. B. Rogers

Acquisition of data (provided animals, acquired and managed patients, provided facilities, etc.): D. B. Darr, J. L. Jordan, C. M. Santos, M. Ross, A. Valdivia, C. R. Miller

Analysis and interpretation of data (e.g., statistical analysis, biostatistics, computational analysis): G. Song, D. B. Darr, B. R. Midkiff, S. Cohen, N. N. Feinberg, T. K. Tarrant, A. B. Rogers, A. C. Dudley, C. M. Perou, W. C. Zamboni

Writing, review, and/or revision of the manuscript: G. Song, D. B. Darr, C. M. Ross, M. Ross, A. Valdivia, J. L. Jordan, B. R. Midkiff, S. Cohen, N. N. Feinberg, C. R. Miller, T. K. Tarrant, A. B. Rogers, A. C. Dudley, C. M. Perou, W. C. Zamboni

Administrative, technical, or material support: D. B. Darr, C. M. Ross, M. Ross, A. Valdivia, J. L. Jordan, B. R. Midkiff, S. Cohen, N. N. Feinberg, C. R., A. B. Rogers, A. C. Dudley

Study supervision: C. M. Perou, W. C. Zamboni

Acknowledgment. The authors would like to thank the North Carolina Translational and Clinical Sciences Institute (NC TraCS) for its support, NC TraCS Biostatistics Core for its review and consultation on study design and statistical analysis, the UNC Lineberger Comprehensive Cancer Center's Mouse Phase I Unit (MP1U) for provision and housing of mouse models, the UNC Animal Clinical Chemistry and Gene Expression Laboratories for their assistance with multiplex chemokine assay, and the UNC Animal Studies Cores for their assistance with the PK and efficacy studies. The authors thank Certara, as a member of the Pharsight Academic Center of Excellence Program, for providing Phoenix WinNonlin software to the Division of Pharmacotherapy and Experimental Therapeutics, UNC Eshelman School of Pharmacy.

REFERENCES

1. Farokhzad OC, Langer R. Impact of nanotechnology on drug delivery. ACS nano. 2009;3(1):16-20.
2. Peer D, Karp JM, Hong S, Farokhzad OC, Margalit R, Langer R. Nanocarriers as an emerging platform for cancer therapy. Nature nanotechnology. 2007;2(12):751-60.
3. Maeda H, Greish K, Fang J. The EPR effect and polymeric drugs: A paradigm shift for cancer chemotherapy in the 21st century. In: Polymer Therapeutics II. Springer; 2006. p. 103-21.
4. Zamboni WC. Concept and clinical evaluation of carrier-mediated anticancer agents. Oncologist. 2008;13(3):248-60.
5. Prabhakar U, Maeda H, Jain RK, Sevick-Muraca EM, Zamboni W, Farokhzad OC, et al. Challenges and key considerations of the enhanced permeability and retention effect for nanomedicine drug delivery in oncology. Cancer Res. 2013;73(8):2412-7.
6. Dobrovolskaia MA, McNeil SE. Immunological properties of engineered nanomaterials. Nature Nanotechnology. 2007;2(8):469-78.
7. Zolnik BS, González-Fernández Á, Sadrieh N, Dobrovolskaia MA. Minireview: Nanoparticles and the immune system. Endocrinology. 2010;151(2):458-65.
8. Li S, Huang L. Pharmacokinetics and biodistribution of nanoparticles. Molecular pharmaceutics. 2008;5(4):496-504.
9. La-Beck NM, Zamboni BA, Gabizon A, Schmeeda H, Amantea M, Gehrig PA, et al. Factors affecting the pharmacokinetics of pegylated liposomal doxorubicin in patients. Cancer Chemother Pharmacol. 2012;69(1):43-50.

10. Song G, Wu H, Yoshino K, Zamboni WC. Factors affecting the pharmacokinetics and pharmacodynamics of liposomal drugs. J Liposome Res. 2012;22(3):177-92.
11. Caron W, Song G, Kumar P, Rawal S, Zamboni W. Interpatient pharmacokinetic and pharmacodynamic variability of carrier-mediated anticancer agents. Clinical Pharmacology & Therapeutics. 2012;91(5):802-12.
12. Zamboni WC, Maruca LJ, Strychor S, Zamboni BA, Ramalingam S, Edwards RP, et al. Bidirectional pharmacodynamic interaction between pegylated liposomal CKD-602 (S-CKD602) and monocytes in patients with refractory solid tumors. J Liposome Res. 2011;21(2):158-65.
13. Joyce JA. Therapeutic targeting of the tumor microenvironment. Cancer cell. 2005;7(6):513.
14. Ben-Baruch A. Host microenvironment in breast cancer development: Inflammatory cells, cytokines and chemokines in breast cancer progression-reciprocal tumor–microenvironment interactions. Breast cancer research. 2002;5(1):31.
15. Fidler IJ. Tumor heterogeneity and the biology of cancer invasion and metastasis. Cancer Res. 1978;38(9):2651-60.
16. Perou CM, Sørlie T, Eisen MB, van de Rijn M, Jeffrey SS, Rees CA, et al. Molecular portraits of human breast tumours. Nature. 2000;406(6797):747-52.
17. Jain RK, Stylianopoulos T. Delivering nanomedicine to solid tumors. Nature Reviews Clinical Oncology. 2010;7(11):653-64.
18. Zamboni WC, Strychor S, Joseph E, Walsh DR, Zamboni BA, Parise RA, et al. Plasma, tumor, and tissue disposition of STEALTH liposomal CKD-602 (S-CKD602) and

nonliposomal CKD-602 in mice bearing A375 human melanoma xenografts. Clinical Cancer Research. 2007;13(23):7217-23.

19. Herschkowitz JI, Simin K, Weigman VJ, Mikaelian I, Usary J, Hu Z, et al. Identification of conserved gene expression features between murine mammary carcinoma models and human breast tumors. Genome Biol. 2007;8(5):R76.
20. Usary JE, Zhao W, Darr D, Roberts PJ, Liu M, Balletta L, et al. Predicting drug responsiveness in human cancers using genetically engineered mice. Clinical Cancer Research. 2013.
21. Maroulakou IG, Anver M, Garrett L, Green JE. Prostate and mammary adenocarcinoma in transgenic mice carrying a rat C3 (1) simian virus 40 large tumor antigen fusion gene. Proceedings of the National Academy of Sciences. 1994;91(23):11236-40.
22. Herschkowitz JI, Zhao W, Zhang M, Usary J, Murrow G, Edwards D, et al. Comparative oncogenomics identifies breast tumors enriched in functional tumor-initiating cells. Proceedings of the National Academy of Sciences. 2012;109(8):2778-83.
23. Prat A, Parker JS, Karginova O, Fan C, Livasy C, Herschkowitz JI, et al. Phenotypic and molecular characterization of the claudin-low intrinsic subtype of breast cancer. Breast Cancer Res. 2010;12(5):R68.
24. Harrell JC, Pfefferle AD, Zalles N, Prat A, Fan C, Khramtsov A, et al. Endothelial-like properties of claudin-low breast cancer cells promote tumor vascular permeability and metastasis. Clin Exp Metastasis. 2014;31(1):33-45.
25. O'brien M, Wigler N, Inbar M, Rosso R, Grischke E, Santoro A, et al. Reduced cardiotoxicity and comparable efficacy in a phase III trial of pegylated liposomal

doxorubicin HCl (CAELYX™/Doxil®) versus conventional doxorubicin for first-line treatment of metastatic breast cancer. Annals of oncology. 2004;15(3):440-9.

26. Zamboni W, Edwards R, Mountz J, Eiseman J, Basse P, Zamboni B, et al. The development of liposomal and nanoparticle anticancer agents: Methods to evaluate the encapsulated and released drug in plasma and tumor and phenotypic probes for pharmacokinetic (PK) and pharmacodynamic (PD) disposition. Proceedings of the 2007 NSTI nanotechnology conference; ; 2007.
27. Takahashi O, Komaki R, Smith PD, Jürgensmeier JM, Ryan A, Bekele BN, et al. Combined MEK and VEGFR inhibition in orthotopic human lung cancer models results in enhanced inhibition of tumor angiogenesis, growth, and metastasis. Clinical Cancer Research. 2012;18(6):1641-54.
28. OHNO S, OHNO Y, SUZUKI N, KAMEI T, KOIKE K, INAGAWA H, et al. Correlation of histological localization of tumor-associated macrophages with clinicopathological features in endometrial cancer. Anticancer Res. 2004;24(5C):3335-42.
29. Lewis CE, Pollard JW. Distinct role of macrophages in different tumor microenvironments. Cancer Res. 2006;66(2):605-12.
30. Choi WW, Lewis MM, Lawson D, Yin-Goen Q, Birdsong GG, Cotsonis GA, et al. Angiogenic and lymphangiogenic microvessel density in breast carcinoma: Correlation with clinicopathologic parameters and VEGF-family gene expression. Modern pathology. 2004;18(1):143-52.
31. Pollack VA, Savage DM, Baker DA, Tsaparikos KE, Sloan DE, Moyer JD, et al. Inhibition of epidermal growth factor receptor-associated tyrosine phosphorylation in

human carcinomas with CP-358,774: Dynamics of receptor inhibition in situ and antitumor effects in athymic mice. J Pharmacol Exp Ther. 1999;291(2):739-48.

32. Nedelman JR, Gibiansky E, Lau DT. Applying bailer's method for AUC confidence intervals to sparse sampling. Pharm Res. 1995;12(1):124-8.
33. Vickers AJ. The use of percentage change from baseline as an outcome in a controlled trial is statistically inefficient: A simulation study. BMC Medical Research Methodology. 2001;1(1):6.
34. Soria G, Ben-Baruch A. The inflammatory chemokines CCL2 and CCL5 in breast cancer. Cancer Lett. 2008;267(2):271-85.
35. Willett CG, Boucher Y, di Tomaso E, Duda DG, Munn LL, Tong RT, et al. Direct evidence that the VEGF-specific antibody bevacizumab has antivascular effects in human rectal cancer. Nat Med. 2004;10(2):145-7.
36. Workman P, Aboagye E, Balkwill F, Balmain A, Bruder G, Chaplin D, et al. Guidelines for the welfare and use of animals in cancer research. Br J Cancer. 2010;102(11):1555-77.
37. Choi M, Stanton-Maxey KJ, Stanley JK, Levin CS, Bardhan R, Akin D, et al. A cellular trojan horse for delivery of therapeutic nanoparticles into tumors. Nano letters. 2007;7(12):3759-65.
38. Banciu M, Schiffelers RM, Storm G. Investigation into the role of tumor-associated macrophages in the antitumor activity of doxil. Pharm Res. 2008;25(8):1948-55.
39. Zhao G, Rodriguez BL. Molecular targeting of liposomal nanoparticles to tumor microenvironment. International journal of nanomedicine. 2013;8:61.

40. Storm G, Steerenberg P, Emmen F, van Borssum Waalkes M, Crommelin D. Release of doxorubicin from peritoneal macrophages exposed in vivo to doxorubicin-containing liposomes. Biochimica et Biophysica Acta (BBA)-General Subjects. 1988;965(2):136-45.
41. Saji H, Koike M, Yamori T, Saji S, Seiki M, Matsushima K, et al. Significant correlation of monocyte chemoattractant protein-1 expression with neovascularization and progression of breast carcinoma. Cancer. 2001;92(5):1085-91.
42. Fang WB, Jokar I, Zou A, Lambert D, Dendukuri P, Cheng N. CCL2/CCR2 chemokine signaling coordinates survival and motility of breast cancer cells through Smad3 protein- and p42/44 mitogen-activated protein kinase (MAPK)-dependent mechanisms. J Biol Chem. 2012;287(43):36593-608.
43. Qian B, Li J, Zhang H, Kitamura T, Zhang J, Campion LR, et al. CCL2 recruits inflammatory monocytes to facilitate breast-tumour metastasis. Nature. 2011;475(7355):222-5.
44. Ma Y, Mattarollo SR, Adjemian S, Yang H, Aymeric L, Hannani D, et al. CCL2/CCR2-dependent recruitment of functional antigen-presenting cells into tumors upon chemotherapy. Cancer Res. 2014 Jan 15;74(2):436-45.
45. Bergers G, Hanahan D. Modes of resistance to anti-angiogenic therapy. Nature Reviews Cancer. 2008;8(8):592-603.
46. Ferrara N. Role of myeloid cells in vascular endothelial growth factor-independent tumor angiogenesis. Curr Opin Hematol. 2010;17(3):219-24.
47. Sahin H, Trautwein C, Wasmuth HE. Functional role of chemokines in liver disease models. Nature Reviews Gastroenterology and Hepatology. 2010;7(12):682-90.
48. Mantovani A. Cancer: Inflammation by remote control. Nature. 2005;435(7043):752-3.

49. Heldin C, Rubin K, Pietras K, Östman A. High interstitial fluid pressure—an obstacle in cancer therapy. Nature Reviews Cancer. 2004;4(10):806-13.

50. Chauhan VP, Stylianopoulos T, Martin JD, Popović Z, Chen O, Kamoun WS, et al. Normalization of tumour blood vessels improves the delivery of nanomedicines in a size-dependent manner. Nature nanotechnology. 2012;7(6):383-8.

FIGURE LEGENDS

Figure 1. Concentration versus time profiles of doxorubicin after administration of PLD or NL-doxo at 6 mg/kg I.V. x 1 via tail vein in (A and B) plasma, (C) tumor, (D) liver, (E) spleen, and (F) lung in basal-like C3-TAg and claudin-low T11 breast tumor models. Samples (n=3 mice at each time point) were obtained at 0.083, 0.5, 1, 3, 6, 24, 48, 72, and 96 hours following PLD or NL-doxo administration. Encapsulated and released doxorubicin after administration of PLD in plasma (B) and sum total (encapsulated and released) doxorubicin in tumor and tissues (C-F) are presented. Each time point is represented as the mean ± standard deviation (SD). *P<0.05 ($AUC_{0\text{-}96h}$ in the C3-TAg model versus $AUC_{0\text{-}96h}$ in the T11 model). Equality of AUC was tested using Nedelman's modification of the Bailer method for sparse samples, using a two-sample test (32). LLOQ for encapsulated doxorubicin: 300 ng/mL, released doxorubicin: 10 ng/mL, and sum total doxorubicin in tissue: 10 ng/g. NL-doxo= NL-doxorubicin. LLOQ= lower limit of quantification.

Figure 2. Hematoxylin & Eosin (H&E), and immunostaining of F4/80, Collagen IV, and CD31 in tumors from basal-like C3-TAg and claudin-low T11 breast tumor models. Representative staining of tumors (brown staining in positive cells) at baseline in the C3-TAg and the T11 models are shown. (A) Representative C3-TAg tumor sections stained for (i) H&E, (ii) F4/80, (iii) Collagen IV and (iv) CD31. (B) Representative T11 tumor sections stained for (i) H&E, (ii) F4/80, (iii) Collagen IV and (iv) CD31. (C) Digital images of (i) F4/80-, (ii) Collagen IV-, and (iii) CD31-stained T11 tumor sections after analysis using the Aperio Membrane v9 algorithm and color deconvolution methods for F4/80 and Collagen IV, respectively, and the Definiens Tissue Studio software for CD31. The markup images of (i) F4/80 and (ii) collagen IV highlight the staining which is color-coded according to their cell classification based on staining intensity (blue= undetectable, yellow= weak, orange= medium, and red= strong). The image of (iii) CD31 highlights the staining which is color-coded based on the size of the detected vessels (yellow=small, orange=intermediate, and red=large). The vascular size was defined as small < 40 μm^2, medium 40 $\mu m^2 \leq$ and < 400 μm^2, and large ≥ 400 μm^2. Digital image of each stained slide was scanned using the Aperio ScanScope XT at an apparent 20X magnification.

Figure 3. F4/80 H-score in tumor versus time profiles in basal-like C3-TAg and claudin-low T11 breast tumor models after administration of PLD or NL-doxo at 6 mg/kg I.V. x 1 via tail vein. F4/80 H-score over time in the C3-TAg tumors following (A) NL-doxo and (B) PLD administration. F4/80 H-score over time in the T11 tumors following (C) NL-doxo and (D) PLD administration. NL-doxo and PLD affected the infiltration of TAMs over time in a drug- and tumor type-dependent manner. Each time point is represented as mean ± SD (n=3). Capsule: Peritumoral/Peripheral tumor; Viable tumor: Intratumoral viable tumor; Necrotic: Intratumoral necrotic tumor. NL-doxo= NL-doxorubicin. TAMs= tumor-associated macrophages.

Figure 4. Profiling of CC chemokine ligands (CCL)2 and CCL5 in basal-like C3-TAg and claudin-low T11 breast tumor models after administration of PLD or NL-doxo at 6 mg/kg I.V. x 1 via tail vein. (A) Intratumoral CCL2 concentrations versus time profiles and (B) plasma CCL2 concentration versus time profiles after PLD or NL-doxo administration in the C3-TAg and the T11 models. The baseline intratumoral expressions of CCL2 were significantly higher in the T11 compared to the C3-TAg ($P<0.0001$). PLD strongly induced the secretion of CCL2 over 96 h in the C3-TAg ($P=0.07$) and the T11 tumors ($P=0.05$) when compared to the slightly increased CCL2 secretion after NL-doxo administration in both models. In plasma, baseline CCL2 concentrations were 2-fold higher in the T11 model compared to the C3-TAg model ($P=0.19$). Plasma CCL2 concentration was significantly increased at 96 h after PLD in the C3-TAg model ($P=0.02$), but little was changed in the T11 model. (C) Intratumoral CCL5 concentrations versus time profiles and (D) plasma CCL5 concentrations versus time after PLD or NL-doxo administration in the C3-TAg and the T11 models. There was no difference in the baseline intratumoral CCL5 concentrations between the two models. After PLD administration, T11 tumors showed significantly increased CCL5 concentrations at 96 hour ($P=0.002$), but a high variability was observed at 96 hour in the C3-TAg model ($P=0.24$). In plasma, the baseline CCL5 concentrations were similar between the two models and little change was observed after PLD or NL-doxo administration in both models. Data are presented as mean ± SEM (n=3 per each time point). *P*-values were calculated using *t*-test for the baseline comparison and for the change from baseline to 96 h after PLD or NL-doxo administration.

Figure 5. The amount of vasculature and the levels of VEGF-a and VEGF-c in basal-like C3-TAg and claudin-low T11 breast tumor models at baseline and at 96 h after administration of PLD or NL-doxo at 6 mg/kg I.V. x 1 via tail vein. (A) MVD score (number of CD31-positive objects per unit area) at baseline in the C3-TAg and the T11 tumors. The T11 tumors had a significantly greater amount of the blood vessel endothelial cells (BECs) compared to the C3-TAg tumors (P=0.04). BECs in the tumor capsule and the viable tumor were assessed for analysis. (B) Open lumen analysis of baseline tumor blood vessels in the C3-TAg and the T11 tumors showed a significantly higher number of blood vessels with lumen in the T11 tumors compared to the C3-TAg tumors (P=0.01). MVD score at baseline and at 96 h after NL-doxo or PLD in (C) the C3-TAg and (D) the T11 tumors. Note that there was little change in the amount of the vasculature in the C3-TAg tumors after NL-doxo or PLD, but a 30% decrease in the MVD score was observed in the T11 tumors after PLD administration. Five most vascularized areas within the tumors ('hotspot'/0.74 mm^2) were chosen for evaluation of the presence of lumen in the blood vasculature. Each of these five areas was analyzed and the mean was calculated per slide. Intratumoral concentrations of (E) VEGF-a and (F) VEGF-c versus time profiles after PLD or NL-doxo in the C3-TAg and the T11 tumors. T11 tumors had significantly higher levels of VEGF-a (P=0.003) and decreased levels of VEGF-c (P=0.03) compared to C3-TAg tumors. PLD had greater impacts on the levels of VEGF-a (P=0.02) and VEGF-c (P=0.02 and P=0.05) compared to NL-doxo and the effects appeared to vary with breast tumor subtypes. Data are presented as mean ± SEM (n=3 or 4). P-values were calculated using unpaired t-test.

Figure 6. Efficacy studies of no treatment, NL-doxo, and PLD in basal-like C3-TAg and claudin-low T11 breast tumor models after administration of PLD or NL-doxo at 6 mg/kg I.V. every week for 6 weeks. Mean tumor growth curves in (A) the C3-TAg and (B) the T11 models. Data are presented as the mean ± SD. Intermediary tumor volumes at (C) 21 days post treatment for the C3-TAg model and at (D) 14 days post treatment for the T11 model. Mean tumor volume comparison indicated that PLD was more efficacious at suppressing tumor growth in the C3-TAg compared to no treatment (P=0.013) and in the T11 compared to no treatment or NL-doxo (P<0.0003 for both). P-values were calculated based on adjusted tumor volume, using analysis of covariance (ANCOVA) followed by adjustment for multiple comparisons using Holm test. Baseline tumor volume was considered as covariate. Kaplan-Meier (KM) analysis of survival after no treatment, NL-doxo, or PLD administration in (E) the C3-TAg and (F) the T11 models was performed. P-values were calculated using two-sided log-rank test. Survival was measured from the first day of drug treatment. 7/7 (no treatment), 17/20 (NL-doxo), and 20/20 (PLD) of the C3-TAg mice were analyzed for the efficacy studies. 11/11 (no treatment), 20/20 (NL-doxo), and 19/20 (PLD) of T11 mice were analyzed for the efficacy studies.

Figure 1

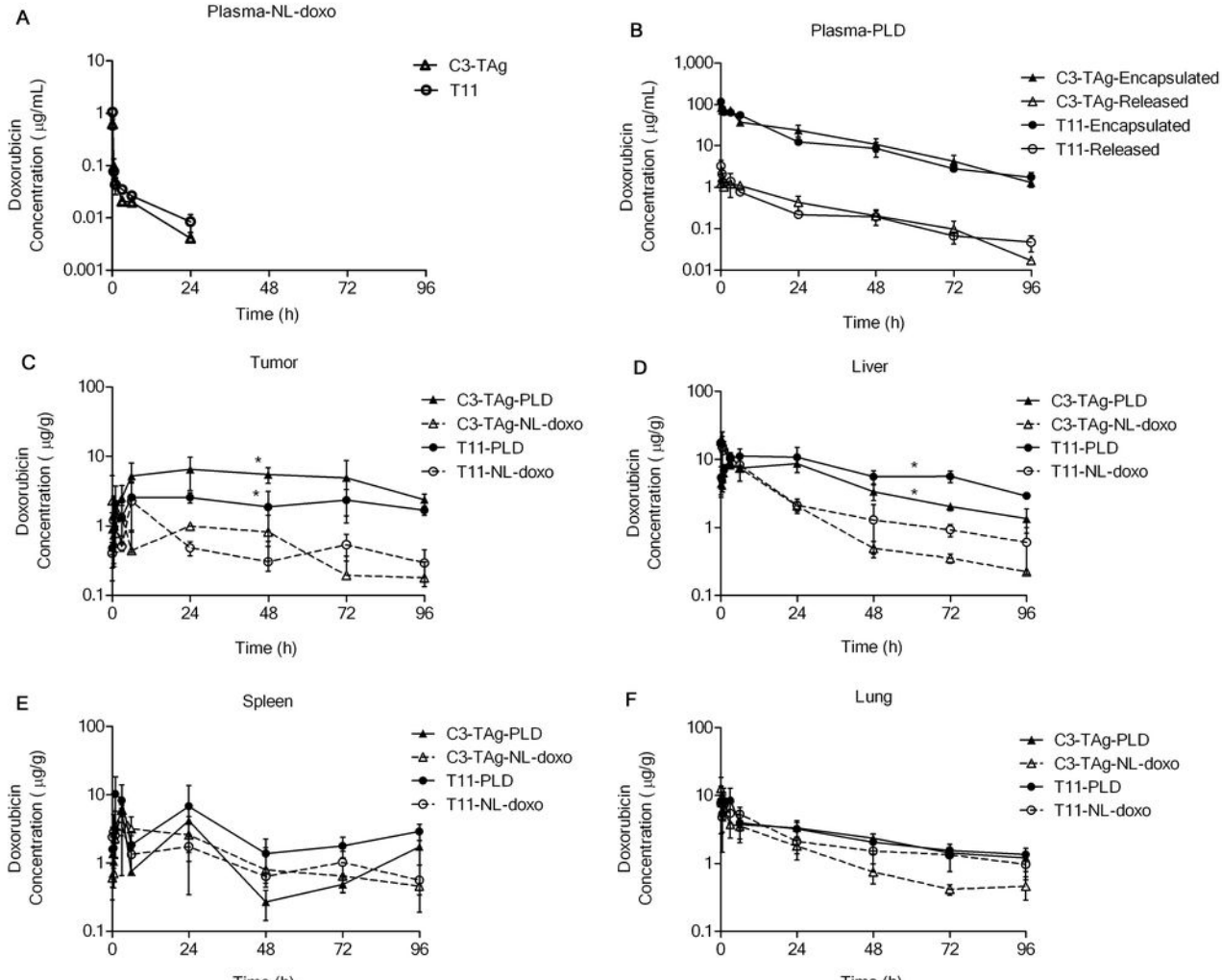

Figure 2

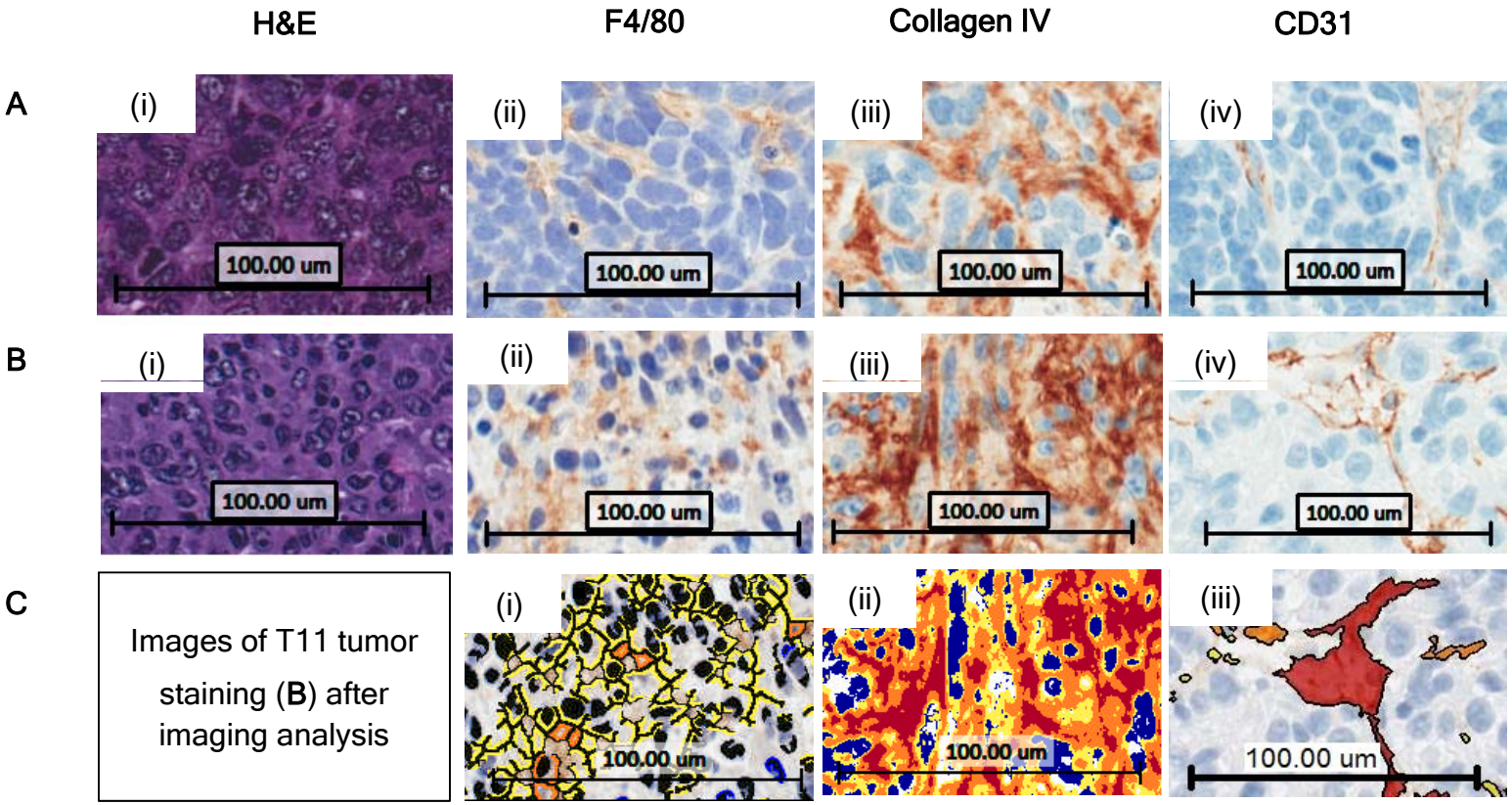

Figure 3

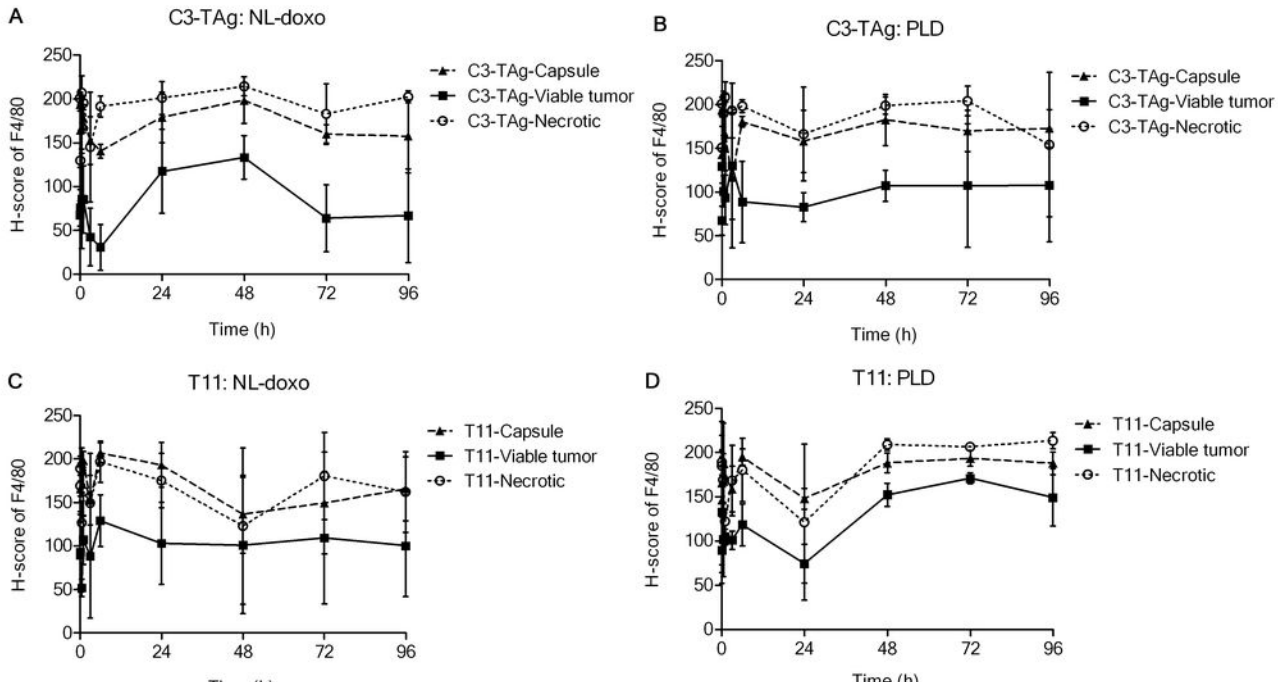

Figure 4

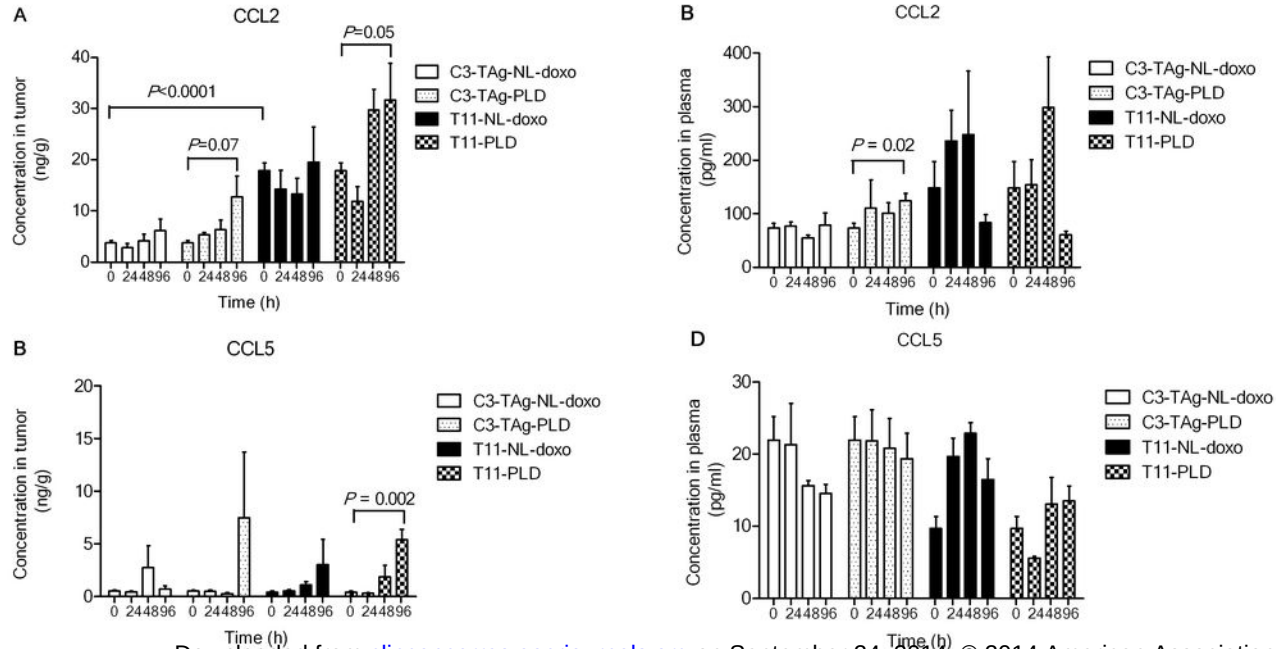

Figure 5

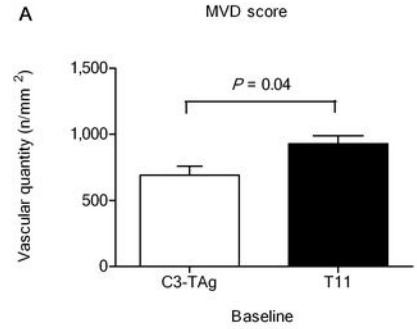

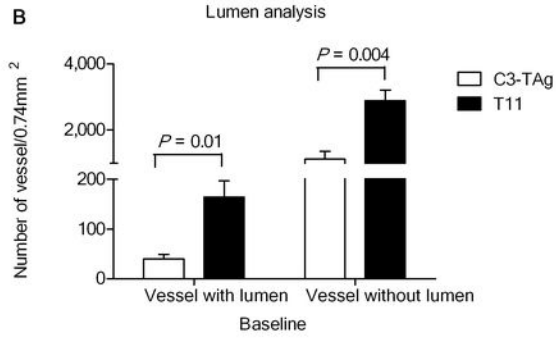

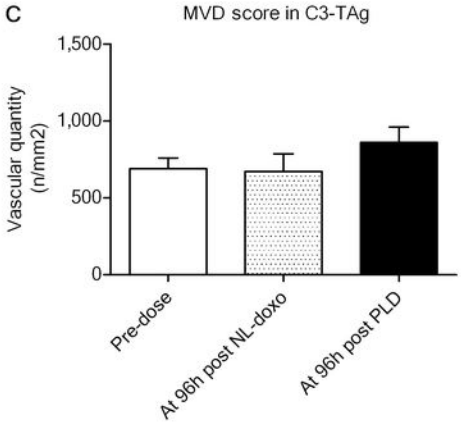

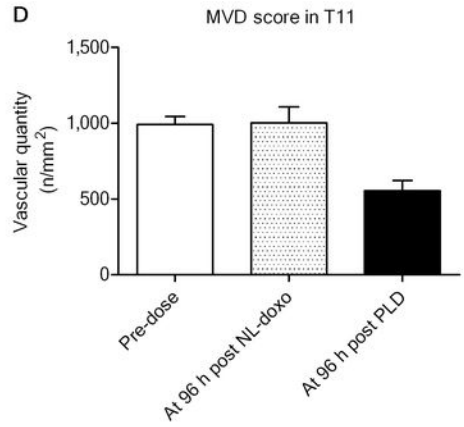

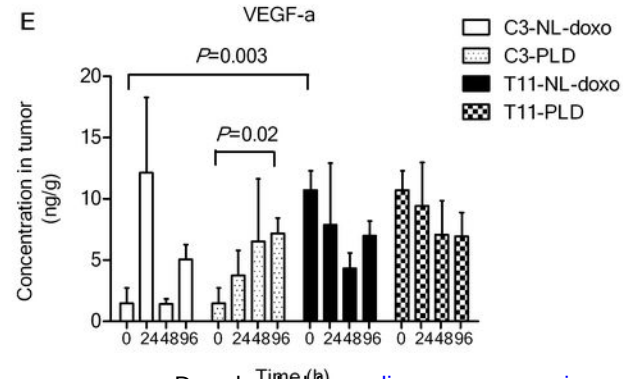

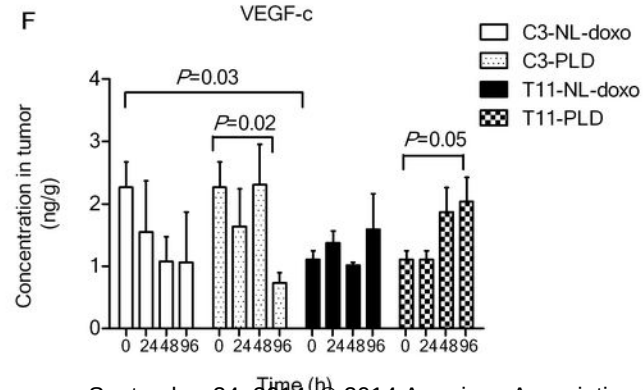

Figure 6